Quaternary Science Reviews 301 (2023) 107930

Contents lists available at ScienceDirect

Quaternary Science Reviews

journal homepage: www.elsevier.com/locate/quascirev

An 1800-year oxygen-isotope record of short- and long-term hydroclimate variability in the northern neotropics from a Jamaican marl lake

Jonathan Holmes [a, *], Michael Burn [b, 1], Luz Maria Cisneros-Dozal [c], Matthew Jones [d], Sarah Metcalfe [d]

[a] Environmental Change Research Centre, Department of Geography, University College London, London, WC1E 6BT, UK
[b] Department of Geography and Geology, The University of the West Indies, Mona Campus, Kingston 7, Jamaica
[c] National Environmental Isotope Facility, Radiocarbon Laboratory, East Kilbride, Scottish Universities Environmental Research Centre, University of Glasgow, G75 0QF, UK
[d] School of Geography, University of Nottingham, Nottingham, NG7 2RD, UK

ARTICLE INFO

Article history:
Received 25 October 2022
Received in revised form
15 December 2022
Accepted 18 December 2022
Available online xxx

Handling Editor: Claudio Latorre

Keywords:
Northern neotropics
Jamaica
Drought
Common era
Stable isotopes
Lake

ABSTRACT

Hydroclimate variability on multi-decadal timescales has been a prominent feature of the circum-Caribbean region over the common era, with marked dry intervals noted in particular for the period 800–950 CE coinciding with the Terminal Classic Period (the so-called Terminal Classic Drought: TCD) in Mesoamerica, and with the Little Ice Age from about 1500 to 1800 CE, linked to complex ocean-atmosphere interactions. Previous compilations of palaeoclimate reconstructions have revealed a clear precipitation dipole between northern and southern Mesoamerica over the common era, which is consistent with meteorological data and modelling experiments. However, patterns of variability elsewhere within the region are less well understood, although palaeoclimate records do point to spatial complexity. Here, we present a ~sub-decadal-scale lake-sediment hydroclimate reconstruction based on ostracod-shell stable isotopes from Wallywash Great Pond, Jamaica, covering the past ~1800 years, which fills a spatial gap in records for the region. Variations in $\delta^{18}O$ values at this site are a proxy for changes in effective moisture and they reveal a marked wet phase over the Terminal Classic Period (TCP), suggesting that the precipitation dipole over northern and southern Mesoamerica may have an east to west component. This is supported by some previous studies, although additional sites are required from strategic localities within the region to confirm this. The Little Ice Age interval at Wallywash is drier than the TCP, although the signal is less clear than at some sites within the wider region, suggesting that regional complexity in hydroclimate has characterised this interval as well.

1. Introduction

Drought has been a striking and recurrent feature of the climate in the Circum-Caribbean region over the past few millennia and multi-year droughts have also been recorded over the last 60 years (Herrera and Ault, 2017). Multiple episodes of drought over extended periods seem to have occurred, most notably during the time from about 800 to 950 CE, which equates to the Terminal Classic Period (TCP) in Mesoamerica (Hodell et al., 1995; Medina-Elizalde et al., 2010; Kennett et al., 2012) as well as during the Medieval Climate Anomaly (MCA: 950–1250 CE. Mann et al., 2009a; Bhattacharya et al., 2017; Wu et al., 2019) and the Little Ice Age (LIA) (Hodell et al., 2005a; Lane et al., 2011a), from around 1500 to 1800 CE.

The climatology of the Caribbean region is complex and a number of different regionalisations have been proposed, some of which also cover the adjacent mainland areas (Jury et al., 2007; Martinez et al., 2019). Jury et al. (2007) note that just focusing on the Caribbean islands reveals patterns that tend to get lost in analyses of the wider region. A range of drivers has been identified, with an emphasis on sea surface temperatures (SSTs) in both the

* Corresponding author.
E-mail address: j.holmes@ucl.ac.uk (J. Holmes).
[1] Present address: School of Biological and Environmental Sciences, Liverpool John Moores University, Liverpool, L3 3AF, UK.

https://doi.org/10.1016/j.quascirev.2022.107930

tropical North Atlantic and Pacific and the position of the North Atlantic Subtropical High (NAH). Strong spatial gradients characterise hydroclimate variability across the region. Most marked of these is a south-north precipitation dipole between southern and northern Mesoamerica, which is expressed in instrumental records of rainfall across the region (Mendez and Magaña, 2010; Herrera and Ault, 2017) reflecting contrasting responses to drivers such as the Atlantic Multidecadal Oscillation (AMO) and El Niño-Southern Oscillation (ENSO). This south-north dipole is also evident in palaeoclimate archives and in model simulations (Stahle et al., 2012; Metcalfe et al., 2015; Bhattacharya and Coats, 2020). It is also seen on an interhemispheric scale over the past millennium (Steinman et al., 2022). An additional, east-west, dipole is also evident in precipitation data (Jury et al., 2007; Martinez et al., 2019; Steiger et al., 2021). However, spatial and temporal patterns of past hydroclimatic variability over the wider region are still not clear, owing to spatial gaps in coverage and dating uncertainties. A clearer picture of such variability is important because it will help to show how hydroclimate responds to various forcing factors and will provide evidence for a better understanding of climatic mechanisms (cf. Konecky et al., 2020).

We present a near-decadal-resolution record of hydroclimate variability for the past 1800 years based on oxygen-isotopes from lake-sediment microfossils from Wallywash Great Pond, SW Jamaica. Located in the western Caribbean Sea, although ~1000 km to the east of the Yucatan Peninsula, the Island of Jamaica is well placed to test models of hydroclimate variability in the wider Caribbean region over the common era. It lies in the driest part of the Caribbean and its present climate is more influenced by ENSO than areas further east (Jury et al., 2007). We compare the Jamaican record with other palaeoclimate time series within the region to investigate spatial patterns of climate variability and to test the hypothesis that an east-west precipitation dipole seen in modern climatological records also prevailed in the region during the equivalent of the Terminal Classic Period and the Little Ice Age (taken here to cover the interval 1500–1800 CE).

The Caribbean region (Fig. 1) is characterised by a seasonal subtropical maritime climate with average temperatures of ~27 °C and a minimum/maximum temperature range of 17–35 °C. The annual precipitation cycle comprises a dry season from December to April and a wet season from May to November and mid-summer drought in July (Taylor et al., 2002; Gamble and Curtis, 2008; Curtis, 2013) and is influenced by thermodynamic and dynamic processes associated with SST variability and regional wind shear, respectively. These, in turn, respond to the seasonal migration of the Hadley Cell and associated changes in the intensity of the Caribbean Low-Level Jet (CLLJ) (Wang, 2007; Cook and Vizy, 2010; Moron et al., 2016), a regional extension of the northeast Trade Winds. During the hurricane season (June–November), precipitation is mostly associated with tropical cyclone activity generated from African Easterly Waves, which are characterised by moist and unstable air masses that move westwards from the African tropics across the region (Landsea, 1993). During the winter dry season, lower SSTs and the southward position of the Hadley Cell (Fig. 1b), enable the subsiding air masses of the NAH to dominate, in turn suppressing rainfall. Rainfall during the boreal winter is mostly localized and associated with the occasional passage of extra-tropical cold fronts (Moron et al., 2016), the frequency of which changes with ENSO state.

On interannual to multidecadal timescales, rainfall is controlled by the relative influence of ENSO, AMO (Klotzbach, 2011) and its close correlative, the Atlantic Meridional Mode (AMM) (Scoccimarro et al., 2018; Jones et al., 2020) and the North Atlantic Oscillation (NAO; Wang, 2007; Wang et al., 2008; Cook and Vizy, 2010; Gouirand et al., 2012). During a developing El Niño event (September–December), positive SST anomalies in the eastern equatorial Pacific increase the surface pressure gradient between the NAH and the Pacific ITCZ strengthening the CLLJ. Enhanced vertical wind shear inhibits the vertical development of convective cells, which suppresses precipitation and storm activity and results in dry conditions across much of the Caribbean, although some increase in winter precipitation from extra-tropical sources occurs in parts of the northwest Caribbean and adjacent mainland areas. In contrast, La Niña-like conditions encourage rainfall and storm activity in the circum-Caribbean and are associated with a weakened

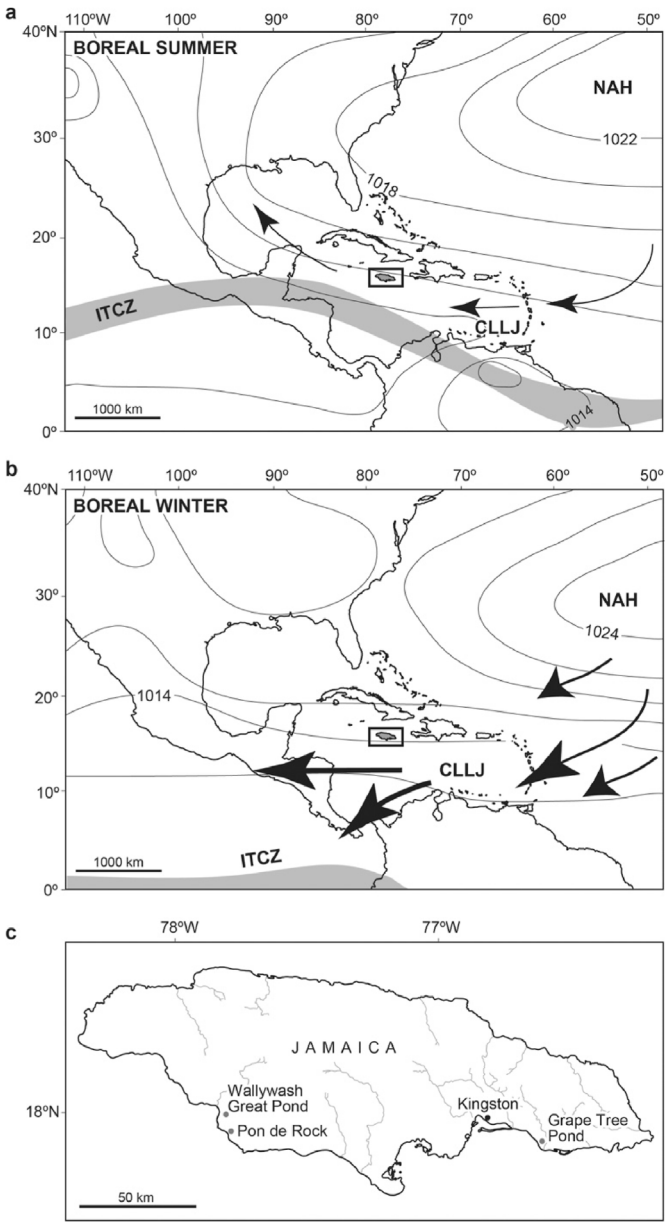

Fig. 1. Regional climate and site location. Atmospheric circulation in the Circum-Caribbean region during (a) boreal summer and (b) boreal winter, adapted from Burn et al. (2016). NAH = North Atlantic Subtropical High Pressure, CLLJ = Caribbean Low-level Jet, ITCZ = Intertropical convergence Zone (location from Asmerom et al., 2020). Rectangle indicates location of Jamaica in (a) and (b). Isobars indicate surface pressure in hectopascals and the thickness of the arrows provides a qualitative indication of relative wind strength. (c) Location of Wallywash Great Pond and other sites in Jamaica that are mentioned in the text.

CLLJ and a low shear-environment, which is conducive to the vertical development of convective cells and thus promotes precipitation.

The Atlantic Multidecadal Oscillation (AMO) influences Atlantic tropical cyclone activity (Goldenberg et al., 2001; Klotzbach, 2011) and precipitation in Africa (Folland et al., 1986; Knight et al., 2006), the Caribbean and circum-Caribbean (Enfield et al., 2001; Stephenson et al., 2014) related to the strength of the CLLJ (Mendez and Magaña, 2010). It is defined by the interdecadal variability in tropical Atlantic SSTs over periods of ~65–70 years (Schlesinger and Ramankutty, 1994) and is clearly recorded in annual resolution coral-based SST reconstructions across the region from Puerto Rico (Kilbourne et al., 2008; Saenger et al., 2009), Venezuela (Hetzinger et al., 2008) and the Caribbean coast of Mexico (Vásquez-Bedoya et al., 2012; Tierney et al., 2015).

The Atlantic Meridional Mode (AMM) is characterised by an anomalous meridional shift in the Intertropical Convergence Zone (ITCZ) that is caused by a warming of SSTs and a weakening of the easterly trade winds in the northern tropical Atlantic (Scoccimarro et al., 2018). When the AMM is positive, the ITCZ and ascending arm of the Hadley cell shift further north, reducing upper-level westerly winds throughout the Atlantic hurricane main development region (MDR). With a negative phase of the AMM, the ascending branch of the Hadley circulation shifts further south, increasing upper-level westerlies and thus increasing westerly shear over the MDR and reducing SSTs. Like the AMO, the AMM has been shown to explain the variability in Atlantic hurricane activity (Vimont and Kossin, 2007) and on multidecadal timescales, covaries significantly with the AMO. Several studies (including Vimont and Kossin, 2007) have suggested that on these longer timescales the AMM may be forced by the AMO.

The NAO affects Caribbean rainfall predominantly during the boreal winter through its influence on the strength and position of the NAH (Wang, 2007; Cook and Vizy, 2010) and in turn the CLLJ. A positive NAO in the boreal winter is characterised by a stronger NAH and CLLJ that combine to cool the ocean surface and advect moisture towards the south-west into the Gulf of Mexico and Central and South America (Martin and Schumacher, 2011). The combination of moisture loss and enhanced surface pressure suppresses atmospheric deep convection causing drier conditions in the circum-Caribbean region. In contrast, during a negative NAO phase, the intensities of the NAH and CLLJ diminish, promoting convective rainfall. However, given that its influence is manifested most strongly during the dry season, which contributes a small percentage of rainfall amounts within the Caribbean, it is thought to exert less control on total mean annual rainfall than ENSO and the AMO. It seems to be more influential in the eastern Caribbean and may enhance or supress ENSO forcing (Giannini et al., 2001).

There is marked spatial heterogeneity in rainfall amount and seasonal cycle across the region (Magaña et al., 1999; Gouirand et al., 2012). Stephenson et al. (2014) subdivided the region into six distinct climatic clusters based on the seasonal rainfall cycle and the timing of the summer precipitation maximum. Jamaica falls into their Zone 2, which is characterised by a distinct bimodal distribution of summer precipitation with peaks in rainfall occurring in May and October separated by a Mid-Summer Drought (MSD) between June and August. This contrasts with rainfall patterns in the Lesser Antilles in the eastern Caribbean, which are dominated by a single late-season maximum in October/November (Jury et al., 2007). Rainfall also varies significantly across Jamaica, with higher amounts occurring in the northeast along the windward side of the Blue Mountains and dry conditions dominating southern areas because of the rain shadow effect. Consequently, most of the rainfall in the southern Parishes of Jamaica occurs during the hurricane season because it is generated by thermodynamic processes associated with warm SSTs and not by trade-wind dominated moisture transport (Burn and Palmer, 2015). Jamaica is affected by tropical weather systems from April to December (metservice.gov.jm), with extra-tropical systems having more influence between January and March. According to Stephenson et al. (2014), Jamaican rainfall is controlled by the varying influence of ENSO and the AMO on interannual to interdecadal timescales.

2. Methods

2.1. Study site

This study is based on stable-isotope data of modern waters and lake-sediment from Wallywash Great Pond (17°57′N, 77°48′W), a small (area = 0.76 km^2), shallow (maximum depth 5 m, mean depth 2.8 m) freshwater karstic lake (Ca–Mg–HCO_3 to Mg–Ca–HCO_3-type) located along the lowland coastal margin of SW Jamaica, close to the town of Black River in the Parish of St Elizabeth (Street-Perrott et al., 1993; Holmes et al., 1995a) (Fig. 1c). The lake lies in a fault-bounded basin in the Oligo-Miocene White Limestone, bordered by the foothills of the Santa Cruz Mountains to the east, which support secondary scrub forest, and by wetland to the north and west (Asprey and Robins, 1953; UNDP/FAO, 1971). The lake catchment experiences a seasonally-wet, tropical climate. Total annual rainfall is 1234 mm at Black River (1901–2016), with large interannual variations but no long-term trend during the 20th and 21st centuries. Most rainfall occurs between May and October, with peak rainfall in those months separated by a drier interval in between. Mean annual air temperature is 26 °C, with little seasonal variation.

Wallywash Great Pond is fed by direct precipitation (~9.33×10^5 m^3 yr^{-1}) and largely-unmonitored springflow from at least two springs (inflow from one of these, the Pumphouse Spring, was ~6.6×10^5 m^3 yr^{-1} in 1966, with little variation through the year: UNDP/FAO, 1971). The main loss is from evaporation (estimated to be ~7.6×10^5 m^3 yr^{-1}, based on a rate of 1000 mm yr^{-1}: Nkemdirim, 1979). A minor amount of water discharges from the northern end of the lake through a small hand-dug channel: any gains and losses from diffuse groundwater flow are un-quantified. Given these values the lake's residence time is around one year. Despite proximity to the coast, the lake does not show significant marine influence (Holmes et al., 1995a). The lake supports well-defined zones of aquatic vegetation (Street-Perrott et al., 1993). Around much of the lake edge is freshwater swamp composed of *Typha, Cyperus* and *Cladium* spp. This is followed by a zone of floating macrophytes including *Nymphaea* and *Nymphoides* spp. and then submerged macrophytes such as *Potamogeton* and *Chara* spp. The lake floor at the northern end is covered with filamentous green algae.

Previous work has demonstrated the suitability of Wallywash Great Pond for palaeoclimatic reconstructions. Street-Perrott et al. (1993) recovered a 9.23 m core (WGP2) from the lake that extended back to ~130 kaBP, and suggested that variations in sediment type (marl, organic marl, lignite and earthy calcareous mud) were related to lake-level changes. They confirmed, using stable-isotope determinations of endogenic carbonate, that the variations in lake level were explained primarily by changes in effective moisture during the late Quaternary. Analyses of inorganic geochemistry (Street-Perrott et al., 1993; Holmes et al., 1995b, 2007) and micropalaeontology (Holmes, 1998) of the core largely supported these findings. However, analyses of core WGP2 were at low temporal resolution (for the Holocene part, typical resolution was 250–350 years) and the age control was subject to large uncertainties. In particular, the analyses were at too low a resolution

and had insufficient age control to be suitable for investigating patterns of climate shift across the wider circum-Caribbean region during the Late Holocene. We therefore collected a new core from the northern basin of the lake, close to the site of WGP2, but focusing on what was likely to be the last ~2000 years of the sequence. Analyses were undertaken at finer stratigraphical intervals than on WGP2, and improvements made to the chronology.

2.2. Water sampling and analysis

Water samples from the lake, groundwater and precipitation (Fig. 2b) were collected at approximately monthly intervals to aid interpretation of the lake-sediment records. Lake waters and shallow groundwater samples were collected by completely filling 30 mL polyethylene bottles, which were then sealed with electrical tape to prevent evaporation. Integrated samples of total monthly rainfall were collected following IAEA protocols (IAEA/GNIP, 2014), in a specially-adapted rainfall collector located at Pon de Rock Guest House (lat: 17.9156°; long: 77.7973°), around 6 km south of Wallywash Great Pond (Fig. 1c). Additional rainwater samples were collected every few hours from 2 to 5 October, 2016 at Kingston (Fig. 1) during the passage of Hurricane Matthew, to characterise the stable isotope composition of rainfall during a hurricane event. Stable isotopes of oxygen and hydrogen were determined simultaneously using a 'Picarro' WS-CRDS system at the University of Liverpool or the University of Cambridge and the results reported in standard delta units relative to the VSMOW standard with 1σ uncertainty of better than 0.07‰ and 0.57‰ for $\delta^{18}O$ and $\delta^{2}H$, respectively.

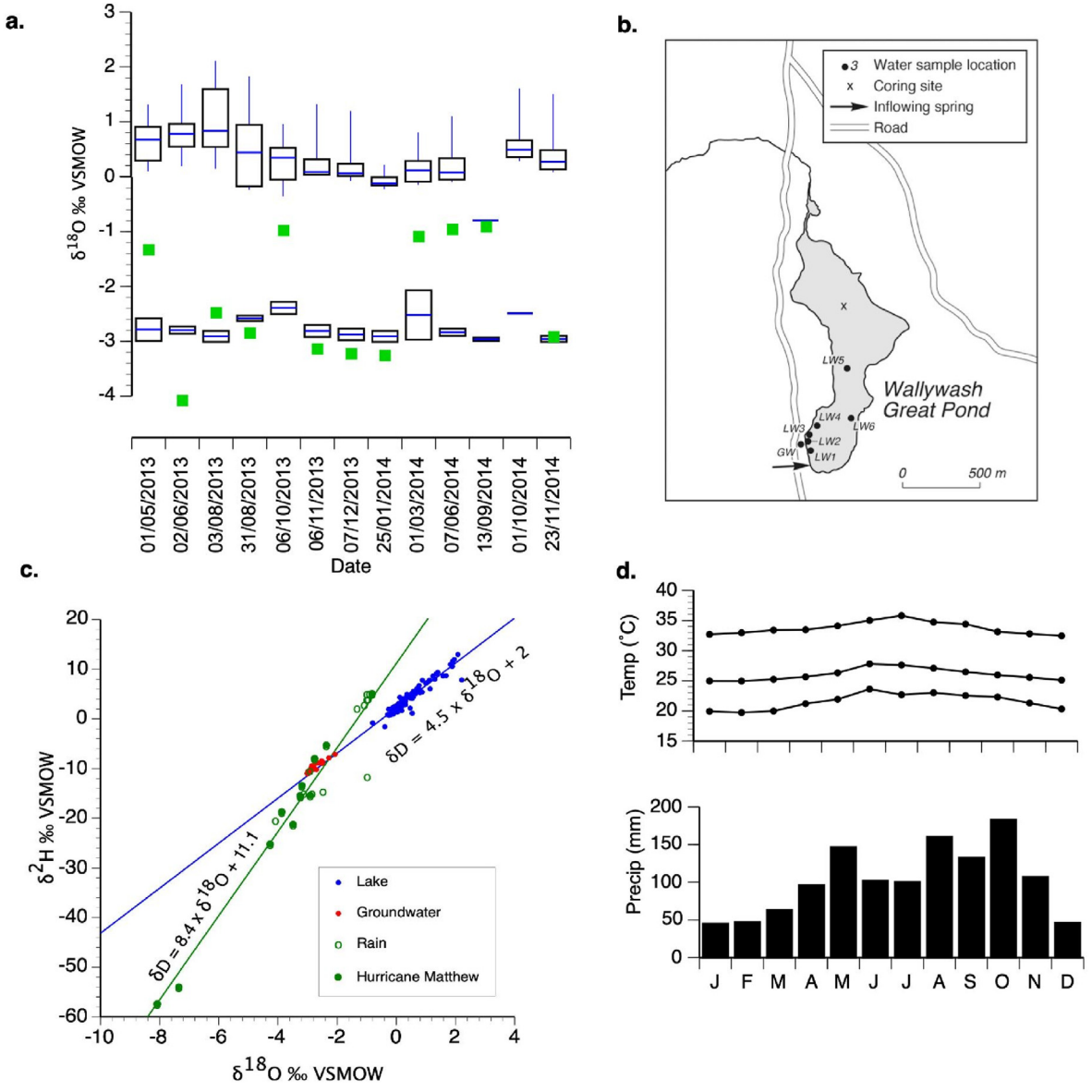

Fig. 2. Modern water isotope data and climate data from Jamaica. (a) Near-monthly variations in oxygen-isotope values of lake water (upper boxes), groundwater (lower boxes) and precipitation (green squares) in 2013–2014. (b) Location of sampling sites on Wallywash Great Pond. LW = lake water, GW = groundwater (c) $\delta^{2}H - \delta^{18}O$ plot of Wallywash Great Pond lake water, groundwater and monthly rainfall measured in 2013–2014. Monthly rainfall was measured at Pon de Rock, 6 km SE of Wallywash Great Pond and rainfall during Hurricane Matthew was measured at Kingston (Fig. 1c) from 2 to October 5, 2016. (d) Monthly temperature and precipitation from Barton Isles (2010–2016) and Black River (1901–2017), respectively (source: Meteorological Service of Jamaica). (For interpretation of the references to colour in this figure legend, the reader is referred to the Web version of this article.)

2.3. Core recovery and analyses

2.3.1. Coring and core description

A 2.16 m sediment core estimated to represent at least the last ~2000 years was recovered in August 2013 from Wallywash Great Pond (Core WAGP; 17°58′20.82″ N; 77°48′27.42″W: Fig. 2b) through 3.15 m of water from an anchored floating platform using a 5 cm diameter Colinvaux–Vohnout drop hammer modified piston corer (Colinvaux et al., 1999). A 52 cm surface core of adjoining unconsolidated sediments deposited below the sediment-water interface was collected using a clear Perspex® tube fitted with a piston, extruded at 1-cm intervals in the field and stored in Whirl-pak® bags. Sediment cores and extruded samples were stored at 4 °C at the Department of Geography, University College London. Visual description of the core was undertaken in the laboratory and complemented by determinations of loss-on-ignition of dried (105 °C overnight) sediment at 550 °C and 950 °C to estimate the organic carbon and carbonate content, respectively (Dean, 1974), performed on every other 1 cm increment of the core.

2.3.2. Chronology

A chronology for core WAGP was produced using a combination of ^{210}Pb and radiocarbon (^{14}C) dating. Dried sediment samples from the uppermost 29 cm of the surface core were used for ^{210}Pb analysis by direct gamma assay in the Environmental Radiometric Facility at University College London. Thirteen radiocarbon dates were produced at various levels from ~45 cm downcore. Plant remains (seeds, carbonized wood fragments) and charcoal fragments were selected for ^{14}C dating by accelerator mass spectrometry at the KECK CCAMS Facility in the University of Irvine, California and at the SUERC AMS Facility, East Kilbride. To avoid interference from old carbonates (^{14}C-depleted, potentially derived from catchment limestone), efforts were made to select plant macrofossils from terrestrial plants or, in the absence of these, plants utilizing primarily atmospheric CO_2 (e.g. from swamp habitats) for ^{14}C dating. Most of the macrofossils identified as probably being from plants utilizing primarily atmospheric CO_2 were paired with samples of charcoal/carbonized wood (collected from the same depth). Only one sample (~45 cm depth) was identified as possibly being from emergent macrophytes although this identification was uncertain (Table 1). The age-depth model, which incorporated all of the ^{210}Pb and ^{14}C ages, was generated in OxCal v4.4 (Bronk Ramsey, 2009a) using the IntCal20 atmospheric calibration curve (Reimer et al., 2020) and the Bayesian deposition model *P-Sequence* (Bronk Ramsey, 2008) with outlier analysis (Bronk Ramsey, 2009b).

2.3.3. Ostracod extraction and isotope analysis

The entire length of core WAGP was processed for ostracod extraction at contiguous 1 cm intervals. For each level, a ~2 cm^3 sample of wet sediment was dispersed in deionised water, sieved through a 250 μm mesh and the >250 μm fraction dried at 40 °C. Fully-calcified adult shells *of Cypretta brevisaepta* were picked from this coarse fraction and cleaned using a 4/0 nylon paint brush and methanol to remove adhering sediment. Oxygen- and carbon-isotope analyses of carbonate (^{18}O/^{16}O, ^{13}C/^{12}C) were undertaken on multiple-shell (typically 5 valves) samples at the Bloomsbury Environmental Isotope Facility (BEIF) in University College London (UCL) using a ThermoFinnigan Delta Plus XP mass spectrometer connected to a GasBench. Isotope values are reported in standard delta notation relative to the VPDB standard, with 1σ uncertainty of better than 0.10‰ and 0.05‰, for oxygen and carbon, respectively.

3. Results

3.1. Modern water isotopes

For the period from May 2013 to November 2014, δ^{18}O values in rainfall ($\delta^{18}O_{ppt}$) varied between −0.9 and −4.1‰ VSMOW, with a mean of −2.1‰. Corresponding values for δ^2H_{ppt} are +5.1‰, −20.1‰ and −6.8‰, respectively. Values for Hurricane Matthew, sampled at Kingston (Fig. 1c) at intervals of several hours between 2 and 5 October 2016, had a lower mean value ($\delta^{18}O_{ppt} = -4.0$‰; $\delta^2H_{ppt} = -22.9$‰) and greater range than the monthly rainfall samples (Fig. 2c). The isotopic composition of groundwater ($\delta^{18}O_{ppt} = -2.8$‰; $\delta^2H_{ppt} = -9.8$‰) is similar to that of average precipitation, but with much less monthly variability (Fig. 2a). The $\delta^{18}O_{ppt}$ and δ^2H_{ppt} and groundwater values fall on a local meteoric water line (LMWL) (Fig. 2c).

δ^{18}O and δ^2H values for Wallywash Great Pond ($\delta^{18}O_{lake}$ and δ^2H_{lake}) also vary spatially and temporally and are described by a line with lower gradient than the LMWL (Fig. 2c), consistent with evaporation as reported originally in Holmes et al. (1995a) for waters sampled in 1990. Similarity between the water-isotope values recorded in 1990 and those reported here for 2013–2014 suggest that the lake water isotope composition is in steady state. Carbon-isotope values of TDIC in the open water of Wallywash Great Pond close to the core site measured in 1990 were −0.34 ± 0.07‰ VPDB (Holmes et al., 1995a).

3.2. Core data

The age-depth model for core WAGP (Table 1; Table 2; Fig. 3) shows that the entire 200 cm core covers the past ~3000 calendar years, although the ostracod-bearing section, which is also the best-dated part of the sequence (albeit with relatively large uncertainties prior to 1000 CE) extends back only to around 200 CE (Fig. 4) and we focus attention on this part of the record. Sedimentation rates vary between <0.1 cm yr^{-1} and ~0.3 cm yr^{-1} or more in the upper 20 cm. The inclusion of outlier analysis in the model enabled us to account for potential interference from old carbon on the radiocarbon dates, a plausible scenario given the site characteristics of the catchment. Agreement indices calculated by OxCal, which indicate how well the model agrees with the data and should usually be over 60%, showed good agreement between the model as a whole and the data ($A_{model} = 85$) and between individual dates at a given depth and the model (all indices A>60%).

The core is composed of calcareous organic mud in the lowermost section, from 183 to 92 cm (~80–1440 CE), with bands of pale marl from 122 to 114 cm (~1250–1300 CE) and 109–107 cm (~1330 CE). A unit of reddish marl overlies the calcareous organic mud from 92 to 79 cm (~1440–1550 CE) and is in turn overlain by pale marl from 79 cm to the surface. LOI_{550} values fall from a high of ~80% near the base to about 20% at 110 cm (~1300 CE). They then rise sharply to about 80% above 110 cm, fall and then rise again between 100 and 90 cm (~1370–1450 CE) and then fall to consistently low values of ~10% above 75 cm (~1590 CE) before showing a steady rise to about 40% in the top 20 cm of the sequence (Fig. 4) (post ~1950 CE). LOI_{950} values are strongly anticorrelated with LOI_{550} (Fig. 4). Although LOI values show a reasonable agreement with the visual stratigraphy, high LOI_{950} values (up to 83%) associated with organic mud between 165 and 110 cm (~590–1300 CE) are explained by the shell content (ostracods and gastropods).

Ostracods shells were present in sufficient numbers for isotope

Table 1
Radiocarbon dates from core WAGP.

Sample ID	Depth (cm)	Publication code	Sample type	Conventional ^{14}C age (years BP)	^{14}C enrichment (% modern)	Modelled (BCE/CE) date range (median)	Sigma	$\delta^{13}C_{VPDB}$ (‰)
W_45-46	45.5	UCIAMS-210625	Unidentified, likely from emergent macrophyte	70 ± 60	99.1 ± 0.7	1715 to 1935 (1829)	61	–
W2_45–46_1	97.5	UCIAMS-210626	Charcoal	770 ± 25	90.9 ± 0.3	1245 to 1600 (1386)	99	–
W2_45–46_3	97.5	UCIAMS-229620	Seeds from sedge (potentially Cladium)	820 ± 20	90.3 ± 0.2	1245 to 1600 (1386)	99	–
W2_48–49_1	100.5	UCIAMS-210627	Charcoal and carbonized wood	925 ± 20	89.1 ± 0.2	1219 to 1590 (1365)	99	–
W2_48–49_2	100.5	SUERC-92928	Seeds from sedge (potentially Cladium)	826 ± 37	90.2 ± 0.4	1219 to 1590 (1365)	99	−28
W2_69–70_2	121.5	UCIAMS-210629	Charcoal and carbonized wood	1085 ± 25	87.4 ± 0.3	1104 to 1438 (1251)	86	–
W2_69–70_1	121.5	UCIAMS-229621	Seeds from sedge (potentially Cladium)	1040 ± 15	87.8 ± 0.2	1104 to 1438 (1251)	86	–
W2_89-90	141.5	UCIAMS-210630	Seeds from sedge (potentially Cladium)	1000 ± 25	88.3 ± 0.2	1053 to 1300 (1153)	68	–
W3_1–2_1	144.5	UCIAMS-210631	Charcoal	875 ± 45	89.7 ± 0.4	1049 to 1283 (1137)	65	–
W3_1–2_2	144.5	UCIAMS-229622	Seeds from herbs/shrubs/succulent (Chenopod)	710 ± 20	91.5 ± 2.2	1049 to 1283 (1137)	65	–
W3_17-18	160.5	UCIAMS-210632	Charcoal and carbonized wood	2455 ± 25	73.7 ± 0.2	234 to 1100 (654)	225	–
W3_37-38	180.5	UCIAMS-210633	Charcoal and carbonized wood	1700 ± 110	81.0 ± 1.0	39 to 700 (363)	163	–
W3_49-50	192.5	SUERC-92929	Seeds from sedge (potentially Cladium)	2956 ± 37	69.2 ± 0.3	−1162 to −884 (−995)	84	−26.1

Table 2
Short-lived radio-isotopes from core WAGP.

Depth	Dry Mass	^{210}Pb						Cumulative Unsupported ^{210}Pb		Chronology		
		Total		Supported		Unsupported						
cm	g cm^{-2}	Bq kg^{-1}	±	Bq kg^{-1}	±	Bq kg^{-1}	±	Bq m^{-2}	±	Date (CE)	Age (aBP)	±
0.5	0.0358	91.38	16.6	72.27	5.91	19.11	17.62	6.6	4.5	2013	0	2
3.5	0.2492	112.91	14.39	75.68	5	37.23	15.23	64.6	27.7	2011	2	2
6.5	0.4304	163.43	19.74	81.44	7.01	81.99	20.95	167.3	42.4	2007	6	3
9.5	0.7077	156.63	18.54	77.7	6.95	78.93	19.8	390.4	68	1998	15	5
11.5	0.9056	149.29	20.39	78.21	7.12	71.08	21.6	538.7	81.2	1989	24	7
12.5	1.0479	152.87	13.47	75.65	4.27	77.22	14.13	644.1	87.2	1981	32	10
13.5	1.1974	161.86	23.07	88.96	7.61	72.9	24.29	756.3	91.1	1970	43	15
14.5	1.3597	114.61	17	86.16	5.72	28.45	17.94	833	98.1	1959	54	21
15.5	1.5275	128.18	12.69	64.8	4.04	63.38	13.32	906.2	102.1	1943	70	26
16.5	1.7525	105.2	9.57	106.48	3.53	−1.28	10.2	976	105.5			
17.5	2.0505	117.03	11.75	105.83	4.28	11.2	12.51	990.8	109.8			
18.5	2.3504	125.12	7.24	110.74	2.56	14.38	7.68	1029	115.1			
20.5	3.0231	113.59	10.73	112.7	3.76	0.89	11.37					
22.5	3.7100	120.57	11.71	125.6	4.22	−5.03	12.45					
26.5	5.1865	97.63	10.32	105.78	3.93	−8.15	11.04					
28.5	5.9542	110.56	6.07	107.35	2.17	3.21	6.45					

analyses above 182 cm in the core, although occurrence is patchy between 182 and 161 cm (~190–650 CE) (Fig. 5). Between 182 and 145 cm (~1120 CE), $\delta^{18}O$ values in ostracods ($\delta^{18}O_{ost}$) are low, with an average around −1.9‰ VPDB and wide variability. $\delta^{13}C_{ost}$ values are also low and variable. Between 144 and 136 cm (~1120–1180 CE), both $\delta^{18}O_{ost}$ and $\delta^{13}C_{ost}$ show positive excursions with amplitude of 6‰ and 8‰, respectively. Between 136 and 100 cm (~1180–1370 CE), $\delta^{18}O_{ost}$ values rise steadily from about −2 to about −0.7‰; $\delta^{13}C_{ost}$ also rise, from about −6 to −4‰. Shorter-term oscillations are superimposed on the general trends for both isotopes. Above 100 cm, the short-term variability in $\delta^{18}O_{ost}$ values decreases as the average $\delta^{18}O_{ost}$ rises to ~0‰ at the core top, consistent with values of −0.24 ± 0.12‰ in living specimens of *Cypretta* collected from the main body of the lake. Negative excursions in $\delta^{18}O_{ost}$ values are evident at 38 and 24 cm (late 19th and early 20th century CE). $\delta^{13}C_{ost}$ values rise sharply by ~6‰ at 100 cm, above which variability is reduced. Living specimens of *Cypretta* collected from the main body of the lake have $\delta^{13}C_{ost}$ values of −0.34 ± 0.07, which are very close to the core-top value of −0.16‰. There is moderate covariance between $\delta^{13}C_{ost}$ and $\delta^{18}O_{ost}$ for the entire record.

4. Discussion

4.1. Intepretation of the stable-isotope records

The oxygen-isotope values of ostracod shells in Wallywash are a function of water temperature and water isotope composition at

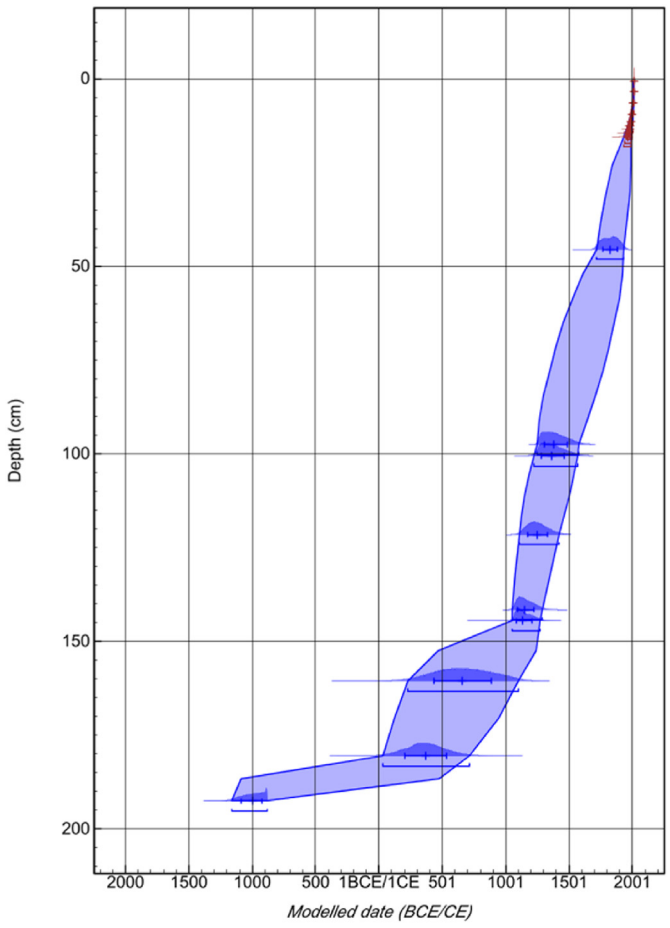

Fig. 3. Age-depth model for core WAGP using ^{210}Pb and ^{14}C dates. The latter were calibrated using the IntCal20 atmospheric calibration curve (Reimer et al., 2020). Model was generated in OxCal v4.4 (Bronk Ramsey, 2009a) using the Bayesian deposition model *P-Sequence* (Bronk Ramsey, 2008) with outlier analysis (Bronk Ramsey, 2009b). Modelled probability at 95% range, probability distributions of ^{210}Pb dates (brown) and ^{14}C dates (blue), median and sigma values shown. (For interpretation of the references to colour in this figure legend, the reader is referred to the Web version of this article.)

the time of shell formation, as well as offset from oxygen-isotope equilibrium, which for *Cypretta brevisaepta* is +1.70 ± 0.22‰ (supplementary information). Little is known about the life cycle of *C. brevisaepta*, but we assume it is a year-round calcifier in tropical lakes owing to minimal seasonal temperature variation, and that the isotopic composition of its shells therefore represents year-round conditions in the lake. The species is regarded as nekto-benthic (Pérez et al., 2010a). However, it is clearly also phytophilous: in Wallywash Great Pond, it is especially abundant amongst the dense stands of submerged macrophytes that are found in the deeper parts of the lake, although it is also present in the shallower margins, and in other smaller freshwater ponds in Jamaica (Holmes, 1997). Notwithstanding taxonomic uncertainties relating to the species (Macario-Gonzalez et al., 2018), these observations are consistent with findings from elsewhere in the neotropics (Pérez et al., 2010b).

It is unlikely that long-term water temperature variations would have had a significant impact on the $\delta^{18}O_{ost}$ values in core WAGP, given the small (<−0.2‰ °C^{-1}) dependence of oxygen-isotope fractionation between water and calcite (Kim and O'Neil, 1997) and modest seasonal and interannual temperature variations in Jamaica. Instead, changes in the isotopic composition of lake water are likely to be the dominant control. The steady-state water-isotope composition (δ_{ss}, modelled in this study for oxygen isotopes) of Wallywash Great Pond was modelled using the equation of Kebede et al. (2002)

$$\delta_{ss} = \frac{\left[\left(\frac{\varepsilon}{h} + \delta_a\right) + \frac{I}{E}\left(\frac{1-h}{h}\right)\delta_i\right]}{\left[1 + \frac{I}{E}\left(\frac{1-h}{h}\right)\right]} \quad (1)$$

where ε = total (kinetic plus equilibrium) fractionation, I = total inflow, E = evaporation, h = relative humidity, δ_i = the oxygen-isotope composition of total inflow and δ_a = the oxygen-isotope composition of atmospheric water vapour, assumed to be in equilibrium with the oxygen-isotope composition of precipitation. For $\delta_i = -2.3‰$, h = 0.8 and T = 28 °C, $\delta_{ss} = +1.7‰$, which is reasonably close to the 2014 average value for the main body of the lake (site LW5; = +1.3 ± 0.6‰).

The steady-state $\delta^{18}O$ value of lake water is sensitive to changes in the oxygen-isotope composition of inflow, to the balance of inflow to evaporation and especially to relative humidity (Fig. 6). In reality, the various factors will interact so that the $\delta^{18}O_{lake}$ and hence $\delta^{18}O_{ost}$ values vary with rainfall amount. Increased rainfall will increase the ratio of inputs to evaporation; it will also lead to lower $\delta^{18}O_{inflow}$ values through the amount effect (Dansgaard, 1964) and decreased kinetic fractionation of lake water because of increased relative humidity. In low latitude regions, the amount effect is often the dominant control on $\delta^{18}O_{ppt}$. Our monitoring data from Jamaica extend over too short a time-period for the amount effect to be shown. However, a strong amount effect is seen in GNIP data from Barbados and the Dominican Republic (IAEA/WMO, 2014), and in investigations of water isotopes from Central America (Lachniet and Patterson, 2002, 2006, 2009). This effect is mostly clearly demonstrated in seasonal data, where its documented effect ranges from −1.24‰ per 100 mm rainfall (Veracruz, Mexico) to −2.93‰ per 100 mm rainfall (Barbados). For long-term data, the effect is much smaller: e.g. −0.12‰ per 100 mm rainfall for Barbados, although the time-series covers only a few years. Neither the long-term nor seasonal amount effect are quantified for Jamaica, but we can reasonably assume that wetter intervals will be associated with decreases in the $\delta^{18}O_{ppt}$, reinforcing the impact of increased P-E on the $\delta^{18}O_{lakewater}$ and hence the $\delta^{18}O_{ost}$.

The carbon-isotope record provides some support for our interpretation of the oxygen-isotope data, even though it is not directly related to hydroclimate. Carbon-isotope values in ostracod shells are determined by the carbon-isotope composition of the dissolved inorganic carbon ($\delta^{13}C_{DIC}$) (Keatings et al., 2002). For *C. brevisaepta* in Wallywash Great Pond, the ostracod shells will record the DIC composition amongst submerged macrophytes during times when the lake was at its deepest, and possibly amongst emergent macrophytes during times of lower lake levels. Here, the DIC signal is most likely reflective of the balance of aquatic photosynthesis to organic decay (Kelts and Talbot, 1990). Photosynthesis involves preferential uptake of ^{12}C, leaving the DIC pool relatively enriched in ^{13}C, whereas decay of organic matter will release ^{12}C-enriched carbon to the DIC pool, as shown by the spatial variations in $\delta^{13}C_{DIC}$ in the modern lake (Holmes et al., 1995a).

4.2. Interpretation of the WAGP record

The earliest part of the WAGP sequence (Fig. 5), from the start of the record until about 1100 CE (146 cm), shows highly variable $\delta^{18}O_{ost}$ values, albeit with low temporal resolution in the first half of the interval. The more negative $\delta^{18}O_{ost}$ equate to a $\delta^{18}O_{lake}$ around 3‰ lower than present assuming unchanged temperature. Although these inferred values are not as low as the $\delta^{18}O$ of modern

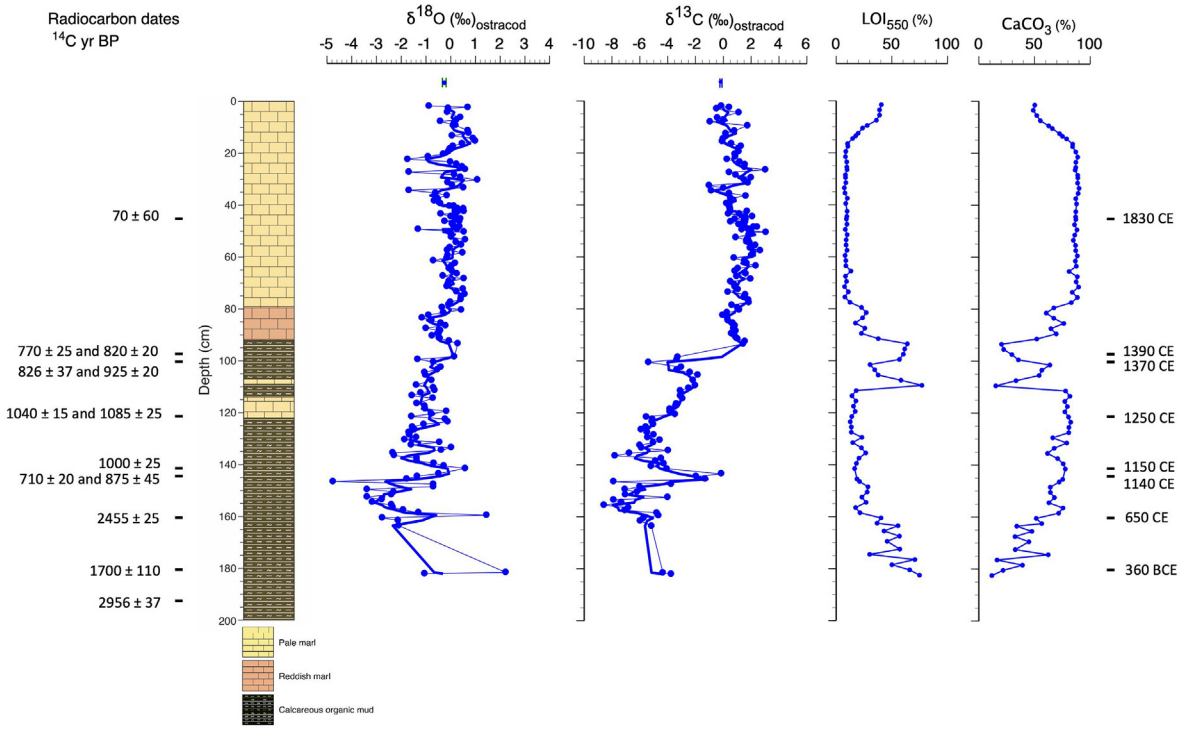

Fig. 4. Core WAGP showing radiocarbon dates, lithostratigraphy, stable-isotope data and loss-on ignition versus core depth. Equivalent median calendar ages (CE/BCE) are shown on the right-hand column. For the oxygen- and carbon-isotope plots, the light line joins the individual datapoints and the heavy line is the 3-point moving average. Stable-isotope datapoints that lie above the main series represent analyses of shells of living specimens of *Cypretta brevisaepta* collected from the main body of the lake (mean ± 1s, n = 4).

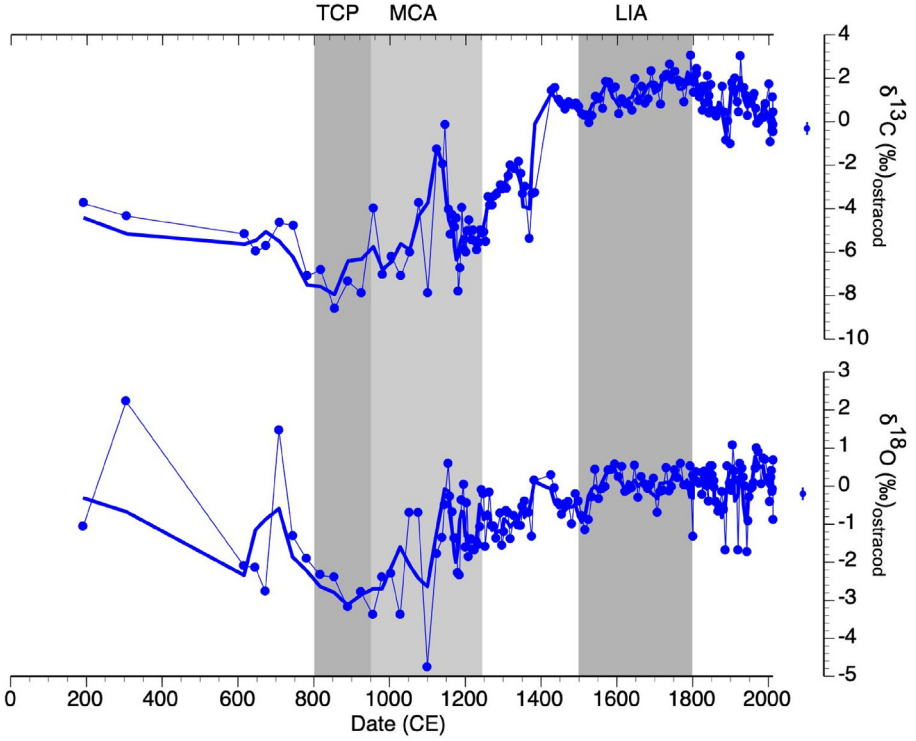

Fig. 5. Stable-isotope data versus age from core WAGP. For both the oxygen- and carbon-isotope plots, the light line joins the individual datapoints and the heavy line is the 3-point moving average. Shaded intervals represent the Terminal Classic Period (TCP), The Medieval Climate Anomaly (MCA) and Little Ice Age (LIA), as defined in the text.

groundwater, they do suggest higher precipitation versus evaporation during this interval compared to later in the record. Low $\delta^{13}C_{ost}$ values accompanying the low $\delta^{18}O_{ost}$ values could be explained by decreased residence time of the lake resulting from

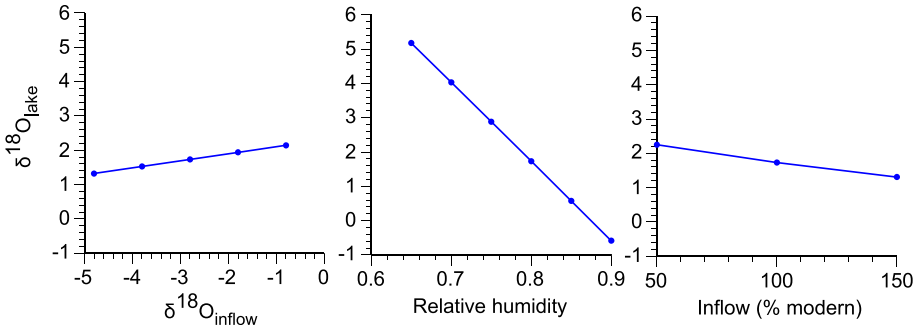

Fig. 6. Sensitivity of Wallywash Great Pond lake water to variations in the $\delta^{18}O$ of input water, relative humidity and variations in the amount of inflow modelled using the equation of Kebede et al. (2002). See text for details of calculations.

increased inputs and outputs, which would reduce the time for the lake's DIC to equilibrate with atmospheric CO_2, or increased contribution of ^{13}C-depleted carbon to the lake from soil-derived organic matter or decay of lacustrine organic matter: both mechanisms operate in Wallywash Great Pond or nearby lakes today (Holmes et al., 1995a). In any case, the carbon-isotope data are consistent with increased effective moisture. There is a positive $\delta^{18}O_{ost}$ excursion around 750 CE and then a short but marked 3–4‰ negative excursion centred on ~1100 CE (~146 cm). The most negative $\delta^{18}O_{ost}$ value is consistent with inferred $\delta^{18}O_{lake}$ up to 5‰ lower than present in the main body of the lake. The negative $\delta^{18}O_{ost}$ excursion is accompanied by reduced $\delta^{13}C_{ost}$. As with the earlier interval, this negative excursion is consistent with increased effective moisture. For the entire part of the record pre-1100 CE, the presence of organic-rich mud in WAGP (Fig. 4) supports this interpretation. The interval from about 750 to 1100 CE is interpreted as a prolonged wet phase, although we acknowledge relatively larger age uncertainties in this part of the record. However, independent sedimentological and stratigraphical evidence from the Black River Morass for a period of enhanced runoff from about 770 to 940 CE (Digerfeldt and Enell, 1984) supports this interpretation. Moreover, the absence of drought indicators and an increase in chlorophyll*a* in Grape Tree Pond, eastern Jamaica (Fig. 1c), is also consistent with wetter conditions then (Heller et al., 2021). Increased frequency and intensity of hurricanes is positively correlated with total annual rainfall amount in Jamaica, at least for much of the 20th century (Burn and Palmer, 2015), and could therefore contribute to the low inferred $\delta^{18}O_{lake}$ values, especially in view of the low $\delta^{18}O_{ppt}$ associated with hurricane rainfall (Fig. 2). An interval of enhanced hurricane activity has been noted for the early part of the Medieval Climate Anomaly (MCA) (Mann et al., 2009b).

In the second interval within WAGP, between 1100 and around 1570 CE (146–77 cm in WAGP), there is a steady rise in $\delta^{18}O_{ost}$ values, with shorter-term ~1‰ oscillations especially in the earlier part. This pattern is also seen in $\delta^{13}C_{ost}$ values, albeit with an increase that is sharper than that in $\delta^{18}O_{ost}$, centred on 100 cm (~1370 CE). The changes in stable-isotope values are accompanied by an abrupt switch from organic mud to marl at about 117 cm (~1260 CE) followed by a rise in LOI_{950} at 96 cm (~1400 CE) (Fig. 4). These changes collectively suggest an increase in evaporative concentration of the lake driven by decreased effective moisture; a reduction in rainfall amount may also have increased the $\delta^{18}O$ of precipitation inputs via the amount effect. The rise in $\delta^{13}C_{ost}$ values may reflect one or more of: increased residence time as inputs of water increased, and hence greater opportunity for the lake DIC to equilibrate with atmospheric CO_2; reduced contribution of soil-derived carbon to the lake's DIC pool or increased aquatic productivity versus decay of lacustrine organic matter in the more evaporated lake.

After 1570 CE, $\delta^{18}O_{ost}$ values remain high and steady, although with ~1‰ multi-decadal negative excursions in the late-18th to early 19th centuries and a trend to slightly lower $\delta^{18}O_{ost}$ near the top of the sequence. $\delta^{13}C_{ost}$ is similarly high and with short-term variation, although weak $\delta^{18}O_{ost}$ and $\delta^{13}C_{ost}$ covariance in this interval suggests that the changes in the latter may be related to variations in aquatic productivity rather than residence time.

In summary, the WAGP record displays an overall trend from wetter to drier climate over the past millennium, on which are superimposed shorter-term (multi-decadal to centennial) variations in effective moisture. The short-term negative excursions in $\delta^{18}O_{ost}$ could feasibly be explained by intervals of ^{18}O-depletion in intense rainfall from tropical cyclones, as has been noted previously in speleothems from Belize (Frappier et al., 2007), although such signatures would register less clearly in lower-resolution lake-sediment records.

We now compare the WAGP time series with other records of hydroclimate across the circum-Caribbean region, with particular attention on two intervals, namely the so-called Terminal Classic period (~800–1000 CE) and the Little Ice Age (1500–1800 CE). There is abundant palaeolimnological (Hodell et al., 1995, 2005b; Curtis et al., 1996; Rosenmeier et al., 2002), speleothem (Medina-Elizalde et al., 2010; Fensterer et al., 2012; Kennett et al., 2012) and marine (Haug et al., 2003) evidence for drought in Mesoamerica and northern South America during the TCP (Fig. 7), with most of the terrestrial evidence derived from lowland sites. High-resolution records confirm that this was a time of multiple-drought episodes rather than a single prolonged dry interval (Medina-Elizalde et al., 2010). Moreover, some well-dated, high-resolution records actually suggest that the late Terminal Classic (as defined here) was wet, or dry to wet (e.g. Medina-Elizalde et al., 2010; Asmerom et al., 2020) (Fig. 7). It is also worth noting that differing definitions of the timing of the TCP relative to the Medieval Climate Anomaly (MCA) can also blur whether these periods are defined as dry or wet. This interval has been linked to the demise of the Classic Maya civilization in the Yucatan Peninsula. Despite debates over the amount of rainfall reduction during the drought (Medina-Elizalde and Rohling, 2012) and its societal impact (Aimers, 2011; Hodell, 2011), there is no doubt that reduced effective moisture characterised at least part of the Terminal Classic interval. Further north, in northern Mexico and the Southwest USA, the TCP was an interval of wetter climate, indicating the existence of a north-south precipitation dipole over the wider region that has been a prominent feature of the past millennium, associated with

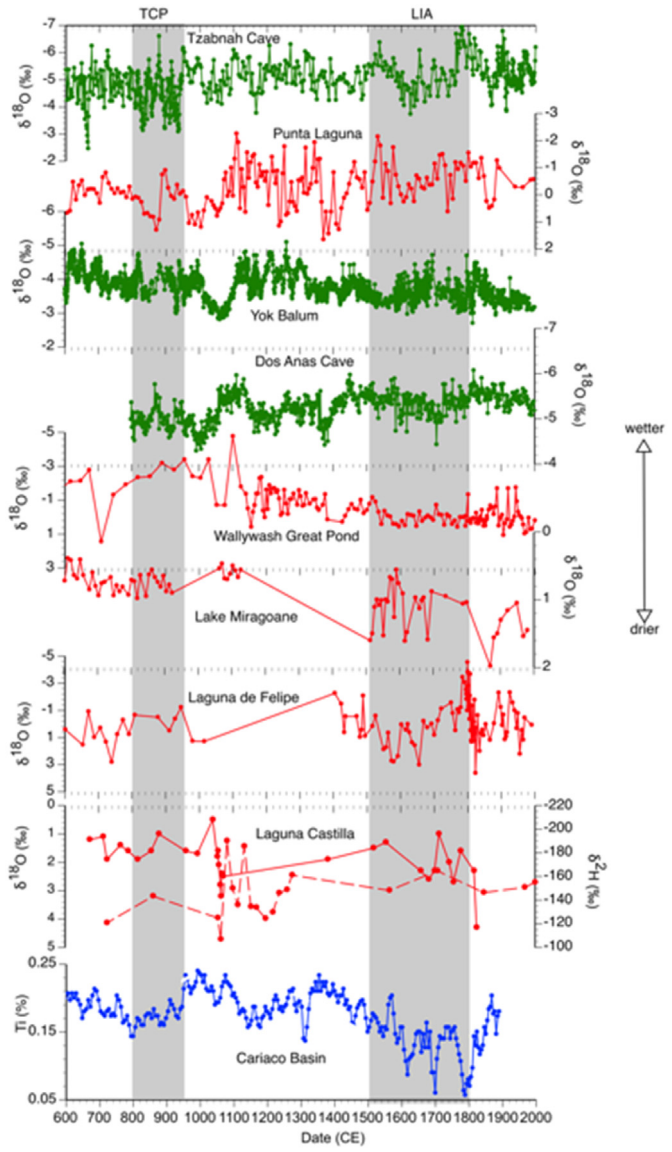

Fig. 7. Comparison of the WAGP record with selected oxygen-isotope records from other lakes and speleothems from the Circum-Caribbean region, and the Cariaco Basin Ti record. Top to bottom (arranged west to east): Chaac speleothem, Tzabnah Cave, Mexico (Medina-Elizalde et al., 2010); Punta Laguna, Yucatan, Mexico (Curtis et al., 1996); Yok Balum speleothem, Belize (Kennett et al., 2012); Dos Anas Cave, Cuba (Fensterer et al., 2012); Wallywash Great Pond (this study); Lake Miragoane, Haiti (Hodell et al., 1991); Laguna de Felipe and Laguna Castilla, Dominican Republic (Lane et al., 2009, 2014); Cariaco Basin (Haug et al., 2003). Shaded intervals represent the Terminal Classic Period (TCP) and Little Ice Age (LIA).

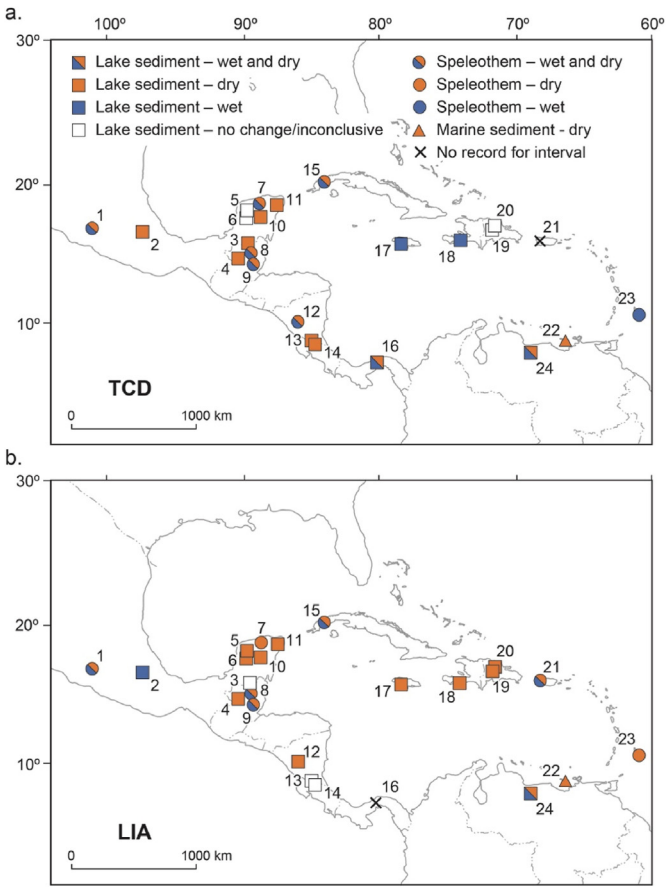

Fig. 8. Qualitative assessment of hydroclimate during (a) the Terminal Classic Drought Period (TCD: defined here as 800–950 CE) and (b) the Little Ice Age (LIA: 1500–1800 CE) in Mesoamerica and the Circum-Caribbean region. Site details are in Table S2. Sites depicted are restricted to those from the northern hemisphere neotropics that also cover the time-periods of interest (i.e. the TCD and LIA).

changes in North Atlantic temperatures, the position of the NAH and gradients of sea-surface temperature between the Pacific and Atlantic Oceans (Bhattacharya and Coats, 2020).

Hydroclimate variations in the wider circum-Caribbean region during the TCP remain less well characterised than in Mesoamerica, with limited data and, in some instances, ambiguous results (Figs. 7 and 8). There is some evidence for drier conditions in the eastern Caribbean during the TCP including oxygen-isotope values from land snails in Guadeloupe (Beets et al., 2006), although the radiocarbon dating may be questionable owing to hardwater error. Hodell et al. (1991) identified a dry-wet-dry oscillation in Lake Miragoane, Haiti, with dry conditions reported from about 2500–1700 ^{14}C years BP (~630 BCE to ~ 340 CE) and then marked wet conditions between 1500 and 800 ^{14}C years (~540–~1220 CE), although suggested that for the Terminal Classic Period, the earlier dry interval might be correlative with the so-called Mayan drought on the Yucatan Peninsula, with the age difference being explained by dating uncertainties. However, if the chronology for the Lake Miragoane record is correct, these data would suggest an *increase* in effective moisture over western Hispaniola during the TCP. Speleothem evidence from Barbados (Ouellette, 2013) also supports wetter conditions during this period. Other evidence is more equivocal. Lane et al. (2009, 2011a,b, 2014) present findings that can be interpreted collectively as demonstrating either wet and dry conditions over the TCP in the Dominican Republic, depending on the site and hydroclimate proxy employed. It is possible that the evidence represents a single wet-dry oscillation, although dating uncertainties and alternative interpretations of the hydroclimate proxies make this unclear. The record from Wallywash Great Pond and data from the nearby Black River Morass adds to the evidence for wetter conditions from parts of the Caribbean region during the TCP, although a better-constrained chronology during this period for both sequences would help to further substantiate this. If correct, this evidence may suggest the existence of a west – east precipitation dipole in this region, superimposed on the north-south dipole evidence between the American Southwest and southern Mesoamerica.

In summary, the oxygen-isotope data from Wallywash Great Pond provide evidence for wetter conditions during the TCP

drought that is seen on the Yucatan Peninsula and elsewhere in Mesoamerica. There is evidence for wetter conditions in some other parts of the wider circum-Caribbean region (Fig. 8). In Jamaica, the wetter conditions may have continued into the later MCA (as defined by Mann et al., 2009a).

As noted above, an east-west dipole is evident in instrumental precipitation data (Jury et al., 2007; Martinez et al., 2019). Moreover, such a pattern appears to be present in the PHYDA data assimilation product (Steiger et al., 2021). Wu et al. (2019) have suggested that intervals of drought over the Yucatan Peninsula are coincident with wetter periods elsewhere in the wider Caribbean region and the data we present provide some support for this.

Bhattacharya et al. (2017) attribute drying in Mesoamerica during the TCP primarily to cooling of the surface North Atlantic. During times of negative AMO, lowered North Atlantic SSTs lead to a decrease in atmospheric moisture, reduced convection and a decrease in the frequency of tropical storms. Concurrently, a strengthening of the CLLJ leads to increased moisture transport to Northern Mexico (Mendez and Magaña, 2010). Other mechanisms may also have played a role. For example, a positive phase of NAO leading to strengthening of the NAH increases the NE Trade winds, which further reduces Atlantic SSTs. Increased Pacific – Atlantic temperature gradients during El Niño events also leads to drought over the Caribbean. However, whilst there is strong evidence for ENSO control on hydroclimate in instrumental records, this is less clear in palaeohydrological records (Bhattacharya et al., 2017). Indeed, palaeoclimatic records suggest a decrease in El Niño events during the TCP (Moy et al., 2002) (Fig. 9). Whilst instrumental data and modelling investigations suggest that drought in Mesoamerica is linked primarily to North Atlantic processes, and that these processes can also explain the North-South precipitation dipole, proxy evidence for oceanographical changes in the North Atlantic during the TCP is equivocal (Bhattacharya et al., 2017), albeit with some evidence for negative North Atlantic SST anomalies during the TCD interval (Wang et al., 2017) (Fig. 9). Similarly, records for changes in NAO during the TCP are inconclusive, with some reconstructions (Wassenburg et al., 2013) suggesting NAO positive conditions during the TCP and others NAO negative (Olsen et al., 2012; Baker et al., 2015; Hernandez et al., 2020), although the lack of a very strong signal in either direction suggests that the NAO may not be a major control. An explanation for an E – W component to the N–S precipitation dipole during the TCP is currently lacking although it may relate to competing influences of the tropical Pacific and North Atlantic Oceans, as noted by Jury et al. (2007) for meteorological records in the Circum-Caribbean region. Reconciling the cooler North Atlantic, and the resulting decreased frequency of tropical storms in the region, with wetter conditions over Jamaica at this time remains a challenge.

The post 1500 CE interval in Wallywash is characterised by reduced effective moisture compared to the earlier part of the record, although the Little Ice Age signature is not particularly strong at this site. Grape Tree Pond (Burn and Palmer, 2014; Heller et al., 2021) provides clearer evidence for reduced effective moisture in eastern Jamaica during the Little Ice Age. Elsewhere, sites across the circum-Caribbean region suggest a relatively dry LIA (Hodell et al., 2005b; Lane et al., 2011a; Metcalfe et al., 2015, 2022) although markedly wet conditions are seen in southern Belize (Asmerom et al., 2020) and East Central Mexico (Lozano-Garcia et al., 2007). For Puerto Rico, Donnnelly and Woodruffe (2007) report low hurricane intensity between 1500 and 1700, followed by a marked increase (so possibly dry to wet). The available data indicate marked spatial variability in Little Ice Age hydroclimate but a north to south precipitation dipole nonetheless, although with no clear evidence for an east-west pattern as is seen for the TCP. Studies at more sites across the Caribbean region are required in order to assess fully conditions during this interval.

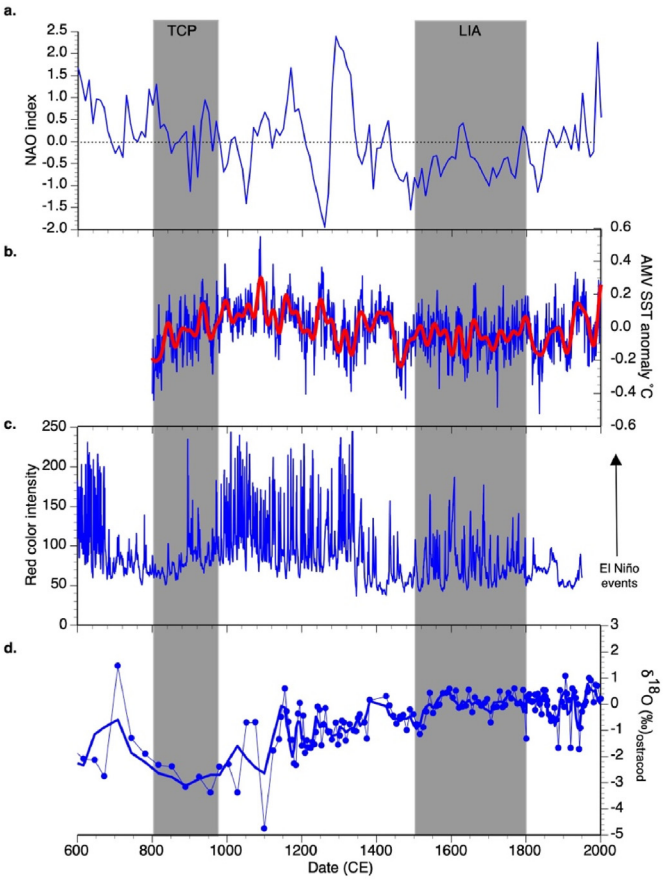

Fig. 9. Climate modes and the oxygen-isotope values from Wallywash Great Pond core WAGP. (a) NAO index from Hernandez et al. (2020). (b) Atlantic multidecadal variability Sea-surface temperature anomaly: blue line shows annually-resolved record and the heavy red line shows 30-year low-pass filter (from Wang et al., 2017). (c) Red colour intensity of sediments from Laguna Pallcacocha, Ecuador, a proxy for El Niño events (Moy et al., 2002). (d) Oxygen-isotope record from Wallywash Great Pond core WAGP (this study). (For interpretation of the references to colour in this figure legend, the reader is referred to the Web version of this article.)

5. Conclusions

We have presented an ostracod-based stable isotope record for the past ~1800 years from southwestern Jamaica. Variations in ostracod $\delta^{18}O$ values are primarily a function of hydroclimate, being driven by changes in effective moisture and rainfall amount. The record shows large and well-defined changes for the past 1800 years with a shift from $\delta^{18}O$ values that are generally more negative prior to about 1000 CE to more positive and less variable after this time, and especially after about 1500 CE. The interval that coincides with the well-studied Terminal Classic Period of the Yucatan Peninsula, which is associated with a well documented dry period in that region, appears to be associated with wet conditions in southwestern Jamaica, as recorded in Wallywash Great Pond and other sites on the island. At Wallywash, wet conditions also appear to have persisted into the early part of the Medieval Climate Anomaly. The interval coinciding with the Little Ice Age is drier than the Terminal Classic interval, although there is a lack of a clear Little

Ice Age signal at Wallywash Great Pond. This lack of a clear signal here is in agreement with some records within the Caribbean region for the LIA, although in contradiction to some other evidence from Jamaica (Burn and Palmer, 2014; Heller et al., 2021).

Evidence for wet conditions during the Terminal Classic Period is found at sites elsewhere in the Caribbean, hinting at the longer-term existence of an east-west precipitation dipole within the region that complements the north – south dipole between southern and northern Mesoamerica. In the both the TCP and the LIA, sea-surface cooling of the tropical North Atlantic, possibly associated with negative phases of the AMO and AMM and a southward displacement of the Atlantic ITCZ (Scoccimarro et al., 2018) may have resulted in drought over southern Mesoamerica and parts of the Caribbean. However, despite the existence of an east-west dipole in some other records, current mechanisms that explain drought in southern Mesoamerica during the TCP coupled with a wet phase to the North, struggle to explain wetter conditions elsewhere in the wider Caribbean region. Further investigations, for example using speleothem archives from strategic locations within the region, are required to confirm this as some of the existing evidence is equivocal. The possible role of the tropical Pacific, specifically ENSO, or ENSO-type variability, in explaining both north - south and east – west dipoles, warrants further study. The potential role of hurricane activity in driving such wetter periods also requires more high-resolution continental records, as well as more SST reconstructions from the key hurricane development region. Such studies will be valuable because they will allow us to test important hypotheses about the long-term behaviour of climate within this complex region and will add to our knowledge of climatic heterogeneity in the past as well as in recent times.

Author contributions

Jonathan Holmes: Conceptualization, Laboratory analyses, Formal analysis, Writing – Original Draft, Visualization, Funding Acquisition. **Michael Burn:** Conceptualization, Fieldwork, Writing – Original Draft**. Luz Maria Cisneros-Dozal:** Laboratory analyses, Formal analysis, Writing – Original Draft, Visualization**. Matthew Jones:** Writing – Review & Editing. **Sarah Metcalfe:** Conceptualization, Formal analysis, Writing – Original Draft, Funding Acquisition.

Declaration of competing interest

The authors declare that they have no known competing financial interests or personal relationships that could have appeared to influence the work reported in this paper.

Data availability

Water-isotope data from Jamaica and lake-sediment data from core WAGP are available from the British Geological Survey (BGS) National Geoscience Data Centre (NGDC) (https://www.bgs.ac.uk/geological-data/national-geoscience-data-centre/)

Acknowledgements

This work was funded by UK NERC Grant 'Neotropics1k' (NE/K00610X/1). We thank Rachel Gwynn and Anne-Lise Jourdan for performing stable isotope analyses, Handong Yang for ^{210}Pb dating, James Shilland for undertaking loss-on-ignition determinations and Miles Irving for drafting figures. Two anonymous reviews helped us to improve the manuscript and are gratefully acknowledged.

Appendix A. Supplementary data

Supplementary data to this article can be found online at https://doi.org/10.1016/j.quascirev.2022.107930.

References

Aimers, J., 2011. FORUM societal collapse drought and the Maya. Nature 479, 44, 44.
Asmerom, Y., Baldini, J.U., Prufer, K.M., Polyak, V.J., Ridley, H.E., Aquino, V.V., Baldini, L.M., Breitenbach, S.F., Macpherson, C.G., Kennett, D.J., 2020. Inter-tropical convergence zone variability in the neotropics during the common era. Sci. Adv. 6, eaax3644. https://doi.org/10.1126/sciadv.aax3644.
Asprey, G.F., Robins, R.G., 1953. Vegetation of Jamaica. Ecol. Monogr. 23, 359–412.
Baker, A., Hellstrom, J.C., Kelly, B.F.J., Mariethoz, G., Trouet, V., 2015. A composite annual-resolution stalagmite record of North Atlantic climate over the last three millennia. Sci. Rep. 5, 10307. https://doi.org/10.1038/srep10307.
Beets, C.J., Troelstra, S.R., Grootes, P.M., Nadeau, M.J., van der Borg, K., de Jong, A.F.M., Hofman, C.L., Hoogland, M.L.P., 2006. Climate and pre-columbian settlement at anse a la Gourde, Guadeloupe, northeastern caribbean. Geo-archaeology-an International Journal 21, 271–280.
Bhattacharya, T., Chiang, J.C.H., Cheng, W., 2017. Ocean-atmosphere dynamics linked to 800-1050 CE drying in Mesoamerica. Quat. Sci. Rev. 169, 263–277.
Bhattacharya, T., Coats, S., 2020. Atlantic-Pacific gradients drive Last Millennium hydroclimate variability in Mesoamerica. Geophys. Res. Lett. 47, e2020GL088061. https://doi.org/10.1029/2020GL088061.
Bronk Ramsey, C., 2008. Deposition models for chronological records. Quat. Sci. Rev. 27, 42–60.
Bronk Ramsey, C., 2009a. Bayesian analysis of radiocarbon dates. Radiocarbon 51, 337–360.
Bronk Ramsey, C., 2009b. Dealing with outliers and offsets in radiocarbon dating. Radiocarbon 51, 1023–1045.
Burn, M.J., Palmer, S.E., 2014. Solar forcing of Caribbean drought events during the last millennium. J. Quat. Sci. 29, 827–836.
Burn, M.J., Holmes, J.A., Kennedy, L.M., Bain, A., Marshall, J.D., Perdikaris, S., 2016. A sediment-based reconstruction of caribbean effective precipitation during the 'little Ice age' from freshwater pond, barbuda. Holocene 26, 1237–1247.
Colinvaux, P.A., De Oliveira, P.E., Moreno, J.E., 1999. Amazon Pollen Manual and Atlas. Hardwood Academic Press, New York.
Cook, K.H., Vizy, E.K., 2010. Hydrodynamics of the Caribbean low-level jet and its relationship to precipitation. J. Clim. 23, 1477–1494.
Curtis, J.H., Hodell, D.A., Brenner, M., 1996. Climate variability on the Yucatan Peninsula (Mexico) during the past 3500 years, and implications for Maya cultural evolution. Quat. Res. 46, 37–47.
Curtis, S., 2013. Daily precipitation distributions over the intra-Americas sea and their interannual variability. Atmósfera 26, 243–259.
Dansgaard, W., 1964. Stable isotopes in precipitation. Tellus 16, 436–468.
Dean, W.E., 1974. Determination of carbonate and organic matter in calcareous sediments and sedimentary rocks by loss of ignition: comparison with other methods. J. Sediment. Petrol. 44, 242–248.
Digerfeldt, G., Enell, M., 1984. Paleoecological studies of past development of the negril and Black River morasses, Jamaica. Appendix 1. In: Björk, S. (Ed.), Environmental Feasibility Study of Peat Mining in Jamaica. Report Prepared for the Petroleum Corporation of Jamaica.
Donnelly, J.P., Woodruff, J.D., 2007. Intense hurricane activity over the past 5,000 years controlled by El Niño and the West African monsoon. Nature 447, 465–468.
Enfield, D.B., Mestas-Nuñez, A.M., Trimble, P.J., 2001. The Atlantic multidecadal oscillation and its relation to rainfall and river flows in the continental US. Geophys. Res. Lett. 28, 2077–2080.
Fensterer, C., Scholz, D., Hoffmann, D., Spötl, C., Pajón, J.M., Mangini, A., 2012. Cuban stalagmite suggests relationship between Caribbean precipitation and the Atlantic Multidecadal Oscillation during the past 1.3 ka. Holocene 22, 1405–1412.
Folland, C.K., Palmer, T.N., Parker, D.E., 1986. Sahel rainfall and worldwide sea temperatures, 1901–85. Nature 320, 602–607.
Frappier, A.B., Sahagian, D., Carpenter, S.J., Gonzalez, L.A., Frappier, B.R., 2007. Stalagmite stable isotope record of recent tropical cyclone events. Geology 35, 111–114.
Gamble, D.W., Curtis, S., 2008. Caribbean precipitation: review, model and prospect. Prog. Phys. Geogr. 32, 265–276.
Giannini, A., Cane, M.A., Kushnir, Y., 2001. Interdecadal changes in the ENSO teleconnection to the caribbean region and the North atlantic oscillation. J. Clim. 14, 2867–2879.
Goldenberg, S.B., Landsea, C.W., Mestas-Nuñez, A.M., Gray, W.M., 2001. The recent increase in Atlantic hurricane activity: causes and implications. Science 293, 474–479.
Gouirand, I., Jury, M.R., Sing, B., 2012. An analysis of low-and high-frequency summer climate variability around the Caribbean Antilles. J. Clim. 25, 3942–3952.
Haug, G.H., Gunther, D., Peterson, L.C., Sigman, D.M., Hughen, K.A., Aeschlimann, B., 2003. Climate and the collapse of Maya civilization. Science 299, 1731–1735.
Heller, C.A., Michelutti, N., Burn, M.J., Palmer, S.E., Smol, J.P., 2021. The response of diatom assemblages in a Jamaican coastal lagoon to hurricane and drought

activity over the past millennium. Holocene 31, 1359–1365.
Hernandez, A., Sanchez-Lopez, G., Pla-Rabes, S., Comas-Bru, L., Parnell, A., Cahill, N., Geyer, A., Trigo, R.M., Giralt, S., 2020. A 2,000-year bayesian NAO reconstruction from the iberian Peninsula. Sci. Rep. 10, 14961. https://doi.org/10.1038/s41598-020-71372-5.
Herrera, D., Ault, T., 2017. Insights from a new high-resolution drought atlas for the Caribbean spanning 1950 − 2016. J. Clim. 30, 7801–7825.
Hetzinger, S., Pfeiffer, M., Dullo, W.C., Keenlyside, N., Latif, M., Zinke, J., 2008. Caribbean coral tracks Atlantic Multidecadal Oscillation and past hurricane activity. Geology 36, 11–14.
Hodell, D., 2011. Maya megadrought? Nature 479, 45.
Hodell, D.A., Curtis, J.H., Jones, G.A., Higuera-Grundy, A., Brenner, M., Binford, M.W., Dorsey, K.T., 1991. Reconstruction of Caribbean climate change over the past 10,500 years. Nature 352, 790–793.
Hodell, D.A., Curtis, J.H., Brenner, M., 1995. Possible role of climate in the collapse of Classic Maya civilization. Nature 375, 391–394.
Hodell, D.A., Brenner, M., Curtis, J.H., Medina-Gonzalez, R., Can, E.I.C., Albornaz-Pat, A., Guilderson, T.P., 2005a. Climate change on the yucatan Peninsula during the little Ice age. Quat. Res. 63, 109–121.
Hodell, D.A., Brenner, M., Curtis, J.H., 2005b. Terminal Classic drought in the northern Maya lowlands inferred from multiple sediment cores in Lake Chichancanab. Quat. Sci. Rev. 24, 1413–1427.
Holmes, J.A., 1998. A late Quaternary ostracod record from Wallywash great pond, a Jamaican marl lake. J. Paleolimnol. 19, 115–128.
Holmes, J.A., Street-Perrott, F.A., Heaton, T.H.E., Darbyshire, D.P.F., Davies, N.C., Hales, P.E., 1995a. Chemical and isotopic composition of karstic lakes in Jamaica, West Indies. Hydrobiologia 312, 121–138.
Holmes, J.A., Street-Perrott, F.A., Ivanovich, M., Perrott, R.A., 1995b. A late Quaternary palaeolimnological record from Jamaica based on trace-element chemistry of ostracod shells. Chem. Geol. 124, 143–160.
Holmes, J.A., Darbyshire, D.P.F., Heaton, T.H.E., 2007. Palaeohydrological significance of late Quaternary strontium isotope ratios in a tropical lake. Chem. Geol. 236, 281–290.
IAEA/WMO 2022. Global Network of Isotopes in Precipitation. The GNIP Database. Accessible at: IAEA/GNIP, 2014. Precipitation Sampling Guide http://www-naweb.iaea.org/napc/ih/documents/other/gnip_manual_v2.02_en_hq.pdf. (Accessed 28 July 2020) https://nucleus.iaea.org/wiser. accessed.
Jones, J.J., Bell, M.M., Klotzbach, P.J., 2020. Tropical and subtropical North Atlantic vertical wind shear and seasonal tropical cyclone activity. J. Clim. 33, 5413–5426.
Jury, M., Malmgren, B.A., Winter, A., 2007. Subregional precipitation climate of the Caribbean and relationships with ENSO and NAO. J. Geophys. Res. 112, D16107. https://doi.org/10.1029/2006JD007541.
Keatings, K.W., Heaton, T.H.E., Holmes, J.A., 2002. Carbon and oxygen isotope fractionation in non-marine ostracods: results from a 'natural culture' environment. Geochem. Cosmochim. Acta 66, 1701–1711.
Kebede, S., Lamb, H., Telford, R., Leng, M., Umer, M., 2002. Lake - groundwater relationships, oxygen isotope balance and climate sensitivity of the Bishoftu Crater Lakes, Ethiopia. In: Odada, E.O., Olago, D.O. (Eds.), The East African Great Lakes: Limnology, Palaeolimnology and Biodiversity. Springer, Dordrecht, pp. 261–275.
Kelts, K., Talbot, M., 1990. Lacustrine carbonates as geochemical archives of environmental change and biotic/abiotic interactions. In: Tilzer, M.M., Serruya, C. (Eds.), Large Lakes: Ecology, Structure and Function, pp. 288–315.
Kennett, D.J., Breitenbach, S.F.M., Aquino, V.V., Asmerom, Y., Awe, J., Baldini, J.U.L., Bartlein, P., Culleton, B.J., Ebert, C., Jazwa, C., Macri, M.J., Marwan, N., Polyak, V., Prufer, K.M., Ridley, H.E., Sodemann, H., Winterhalder, B., Haug, G.H., 2012. Development and disintegration of Maya political systems in response to climate change. Science 338, 788–791.
Kilbourne, K.H., Quinn, T.M., Webb, R., Guilderson, T., Nyberg, J., Winter, A., 2008. Paleoclimate proxy perspective on Caribbean climate since the year 1751: evidence of cooler temperatures and multidecadal variability. Paleoceanography 23. https://doi.org/10.1029/2008PA001598.
Kim, S.T., O'Neil, J.R., 1997. Equilibrium and nonequilibrium oxygen isotope effects in synthetic carbonates. Geochem. Cosmochim. Acta 61, 3461–3475.
Klotzbach, P.J., 2011. The influence of El Niño–Southern Oscillation and the Atlantic multidecadal oscillation on Caribbean tropical cyclone activity. J. Clim. 24, 721–731.
Knight, J.R., Folland, C.K., Scaife, A.A., 2006. Climate impacts of the Atlantic multidecadal oscillation. Geophys. Res. Lett. 33, L17706. https://doi.org/10.1029/2006GL026242.
Konecky, B.L., McKay, N.P., Churakova, O.V., Comas-Bru, L., Dassié, E.P., DeLong, K.L., Falster, G.M., Fischer, M.J., Jones, M.D., Jonkers, L., Kaufman, D.S., Leduc, G., Managave, S.R., Martrat, B., Opel, T., Orsi, A.J., Partin, J.W., Sayani, H.R., Thomas, E.K., Thompson, D.M., Tyler, J.J., Abram, N.J., Atwood, A.R., Cartapanis, O., Conroy, J.L., Curran, M.A., Dee, S.G., Deininger, M., Divine, D.V., Kern, Z., Porter, T.J., Stevenson, S.L., von Gunten, L., Iso2k Project member, 2020. The Iso2k database: a global compilation of paleo-$\delta^{18}O$ and $\delta^{2}H$ records to aid understanding of Common Era climate. Earth Syst. Sci. Data 12, 2261–2288. https://doi.org/10.5194/essd-12-2261-2020.
Lachniet, M.S., Patterson, W.P., 2002. Stable isotope values of Costa Rican surface waters. J. Hydrol. 260, 135–150.
Lachniet, M.S., Patterson, W.P., 2006. Use of correlation and multiple stepwise regression to evaluate the climatic controls on the stable isotope values of Panamanian surface waters. J. Hydrol. 324, 115–140.
Lachniet, M.S., Patterson, W.P., 2009. Oxygen isotope values of precipitation and surface waters in northern Central America (Belize and Guatemala) are dominated by temperature and amount effects. Earth Planet Sci. Lett. 284, 435–446.
Lane, C.S., Horn, S.P., Mora, C.I., Orvis, K.H., 2009. Late-Holocene paleoenvironmental change at mid-elevation on the Caribbean slope of the Cordillera Central, Dominican Republic: a multi-site, multi-proxy analysis. Quat. Sci. Rev. 28, 2239–2260.
Lane, C.S., Horn, S.P., Orvis, K.H., Thomason, J.M., 2011a. Oxygen isotope evidence of little Ice age aridity on the caribbean slope of the cordillera central, Dominican republic. Quat. Res. 75, 461–470.
Lane, C.S., Horn, S.P., Mora, C.I., Orvis, K.H., Finkelstein, D.B., 2011b. Sedimentary stable carbon isotope evidence of late Quaternary vegetation and climate change in highland Costa Rica. J. Paleolimnol. 45, 323–338.
Lane, C.S., Horn, S.P., Kerr, M.T., 2014. Beyond the mayan lowlands: impacts of the terminal classic drought in the caribbean Antilles. Quat. Sci. Rev. 86, 89–98.
Landsea, C., 1993. A climatology of intense (or major) Atlantic hurricanes. Mon. Weather Rev. 121, 1703–1713.
Lozano-Garcia, M.D., Caballero, M., Ortega, B., Rodriguez, A., Sosa, S., 2007. Tracing the effects of the little Ice age in the tropical lowlands of eastern Mesoamerica. Proc. Natl. Acad. Sci. U. S. A 104, 16200–16203.
Macario-Gonzalez, L., Cohuo, S., Elias-Gutierrez, M., Vences, M., Perez, L., Schwalb, A., 2018. Integrative taxonomy of freshwater ostracodes (Crustacea: Ostracoda) of the Yucatan Peninsula, implications for paleoenvironmental reconstructions in the northern Neotropical region. Zool. Anz. 275, 20–36.
Magaña, V., Amador, J.A., Medina, S., 1999. The midsummer drought over Mexico and Central America. J. Clim. 12, 1577–1588.
Mann, M.E., Zhang, Z.H., Rutherford, S., Bradley, R.S., Hughes, M.K., Shindell, D., Ammann, C., Faluvegi, G., Ni, F.B., 2009a. Global signatures and dynamical origins of the little Ice age and medieval climate anomaly. Science 326, 1256–1260.
Mann, M.E., Woodruff, J.D., Donnelly, J.P., Zhang, Z.H., 2009b. Atlantic hurricanes and climate over the past 1,500 years. Nature 460. 880-U115.
Martin, E.R., Schumacher, C., 2011. The Caribbean low-level jet and its relationship with precipitation in IPCC AR4 models. J. Clim. 24, 5935–5950.
Martinez, C., Goddard, L., Kushnir, Y., Ting, M., 2019. Seasonal climatology and dynamical mechanisms of rainfall in the Caribbean. Clim. Dynam. 53, 825–846.
Medina-Elizalde, M., Burns, S.J., Lea, D.W., Asmerom, Y., von Gunten, L., Polyak, V., Vuille, M., Karmalkar, A., 2010. High resolution stalagmite climate record from the Yucatan Peninsula spanning the Maya terminal classic period. Earth Planet Sci. Lett. 298, 255–262.
Medina-Elizalde, M., Rohling, E.J., 2012. Collapse of Classic Maya civilization related to modest reduction in precipitation. Science 335, 956–959.
Mendez, M., Magaña, V., 2010. Regional aspects of prolonged meteorological droughts over Mexico and Central America. J. Clim. 23, 1175–1188.
Metcalfe, S.E., Barron, J.A., Davies, S.J., 2015. The Holocene history of the North American Monsoon: 'known knowns' and 'known unknowns' in understanding its spatial and temporal complexity. Quat. Sci. Rev. 120, 1–27.
Metcalfe, S.E., Holmes, J.A., Jones, M.D., Medina Gonzalez, R., Primmer, N.J., Martinez Dyrzo, H., Davies, S.J., Le, 2022. Response of a low elevation carbonate lake in the Yucatan Peninsula (Mexico) to climatic and human forcings. Quat. Sci. Rev. 282. https://doi.org/10.1016/j.quascirev.2022.107445.
Moron, V., Gouirand, I., Taylor, M., 2016. Weather types across the Caribbean basin and their relationship with rainfall and sea surface temperature. Clim. Dynam. 47, 601–621.
Moy, C.M., Seltzer, G.O., Rodbell, D.T., Anderson, D.M., 2002. Variability of El niño-southern oscillation activity at millennial timescales during the Holocene. Nature 420, 162–165.
Nkemdirim, L.C., 1979. Spatial and seasonal distribution of rainfall and runoff in Jamaica. Geogr. Rev. 69, 288–301.
Olsen, J., Anderson, N.J., Knudsen, M.F., 2012. Variability of the North atlantic oscillation over the past 5,200 years. Nat. Geosci. 5, 808–812.
Ouellette, G.R., 2013. Late Holocene paleoenvironmental reconstruction in Barbados. MS Thesis, Western Kentucky University.
Pérez, L., Lorenschat, J., Bugja, R., Brenner, M., Scharf, B., Schwalb, A., 2010a. Distribution, biodiversity, and ecology of modern freshwater ostracodes (Crustacea), and hydrochemical characteristics of Lago Petén Itzá, Guatemala. J. Limnol. 69, 146–159.
Pérez, L., Lorenschat, J., Brenner, M., Scharf, B., Schwalb, A., 2010b. Extant freshwater ostracodes (Crustacea: Ostracoda) from lago petén itzá, Guatemala. Rev. Biol. Trop. 58, 871–895.
Reimer, P., Austin, W., Bard, E., Bayliss, A., Blackwell, P., Bronk Ramsey, C., Butzin, M., Cheng, H., Edwards, R., Friedrich, M., Grootes, P., Guilderson, T., Hajdas, I., Heaton, T., Hogg, A., Hughen, K., Kromer, B., Manning, S., Muscheler, R., Palmer, J., Pearson, C., van der Plicht, J., Reimer, R., Richards, D., Scott, E., Southon, J., Turney, C., Wacker, L., Adolphi, F., Büntgen, U., Capano, M., Fahrni, S., Fogtmann-Schulz, A., Friedrich, R., Köhler, P., Kudsk, S., Miyake, F., Olsen, J., Reinig, F., Sakamoto, M., Sookdeo, A., Talamo, S., 2020. The IntCal20 Northern Hemisphere radiocarbon age calibration curve (0–55 cal kBP). Radiocarbon 62, 725–757.
Rosenmeier, M.F., Hodell, D.A., Brenner, M., Curtis, J.H., Guilderson, T.P., 2002. A 4000-year lacustrine record of environmental change in the southern Maya lowlands, Peten, Guatemala. Quat. Res. 57, 183–190.
Saenger, C., Cohen, A.L., Oppo, D.W., Halley, R.B., Carilli, J.E., 2009. Surface-temperature trends and variability in the low-latitude North Atlantic since 1552. Nat. Geosci. 2, 492–495.

Schlesinger, M.E., Ramankutty, N., 1994. An oscillation in the global climate system of period 65–70 years. Nature 367, 723–726.
Scoccimarro, E., Bellucci, A., Storto, A., Gualdi, S., Masina, S., Navarra, A., 2018. Remote subsurface ocean temperature as a predictor of Atlantic hurricane activity. Proc. Natl. Acad. Sci. USA 115, 11460–11464. https://doi.org/10.1073/pnas.1810755115.
Stahle, D.W., Burnette, D.J., Villanueva Diaz, J., Heim Jr., R.R., Fye, F.K., Cerano Paredes, J., Acuna Soto, R., Cleaveland, M.K., 2012. Pacific and Atlantic influences on Mesoamerican climate over the past millennium. Clim. Dynam. 39, 1431–1446.
Steiger, N.J., Smerdon, J.E., Seager, R., Williams, A.P., Varuolo-Clarke, A.M., 2021. ENSO-driven coupled megadroughts in North and South America over the last millennium. Nat. Geosci. 14, 739–744.
Steinman, B.A., Stansell, N.D., Mann, M.E., Cooke, C.A., Abbott, M.B., Vuille, M., Bird, B.W., Lachniet, M.S., Fernandez, A., 2022. Interhemispheric antiphasing of neotropical precipitation during the past millennium. Proc. Natl. Acad. Sci. USA 119, e2120015119. https://doi.org/10.1073/pnas.2120015119.
Stephenson, T.S., Vincent, L.A., Allen, T., Van Meerbeeck, C.J., McLean, N., Peterson, T.C., Taylor, M.A., Aaron-Morrison, A.P., Auguste, T., Bernard, D., Boekhoudt, J.R., 2014. Changes in extreme temperature and precipitation in the Caribbean region, 1961–2010. Int. J. Climatol. 34, 2957–2971.
Street-Perrott, F.A., Hales, P.E., Perrott, R.A., Fontes, J.C., Switsur, V.R., Pearson, A., 1993. Late quaternary palaeolimnology of a tropical marl lake: Wallywash great pond, Jamaica. J. Paleolimnol. 9, 3–22.
Taylor, M.A., Enfield, D.B., Chen, A.A., 2002. Influence of the tropical atlantic versus the tropical pacific on caribbean rainfall. J. Geophys. Res.: Oceans 107 (C9), 3127. https://doi.org/10.1029/2001JC001097.
Tierney, J.E., Abram, N.J., Anchukaitis, K.J., Evans, M.N., Giry, C., Kilbourne, K.H., Saenger, C.P., Wu, H.C., Zinke, J., 2015. Tropical sea surface temperatures for the past four centuries reconstructed from coral archives. Paleoceanography 30, 226–252.
UNDP/UNFAO, 1971. Groundwater Surveys in Two Areas of the Interior, Jamaica. Appraisal Report of the Pedro Plains, vol. 1. SF/JAM3 Technical Report, St. Elizabeth. AL, pp. 1–192.
Vásquez-Bedoya, L.F., Cohen, A.L., Oppo, D.W., Blanchon, P., 2012. Corals record persistent multidecadal SST variability in the Atlantic Warm Pool since 1775 AD. Paleoceanography 27, PA3231. https://doi.org/10.1029/2012PA002313.
Vimont, D.J., Kossin, J.P., 2007. The atlantic meridional mode and hurricane activity. Geophys. Res. Lett. 34, GL029683. https://doi.org/10.1029/2007GL029683.
Wang, C., 2007. Variability of the Caribbean low-level jet and its relations to climate. Clim. Dynam. 29, 411–422.
Wang, C., Lee, S.K., Enfield, D.B., 2008. Atlantic warm pool acting as a link between Atlantic multidecadal oscillation and Atlantic tropical cyclone activity. G-cubed 9, Q05V03. https://doi.org/10.1029/2007GC001809.
Wang, J., Yang, B., Ljungqvist, F.C., Luterbacher, J., Osborn, Timothy J., Briffa, K.R., Zorita, E., 2017. Internal and external forcing of multidecadal Atlantic climate variability over the past 1,200 years. Nat. Geosci. 10, 512–517.
Wassenburg, J.A., Immenhauser, A., Richter, D.K., Niedermayr, A., Riechelmann, S., Fietzke, J., Scholz, D., Jochum, K.P., Fohlmeister, J., Schroder-Ritzrau, A., Sabaoui, A., Riechelmann, D.F.C., Schneider, L., Esper, J., 2013. Moroccan speleothem and tree ring records suggest a variable positive state of the North Atlantic Oscillation during the Medieval Warm Period. Earth Planet Sci. Lett. 375, 291–302.
Wu, J., Porinchu, D.F., Horn, S.P., 2019. Late Holocene hydroclimate variability in Costa Rica: signature of the terminal classic drought and the Medieval Climate Anomaly in the northern tropical Americas. Quat. Sci. Rev. 215, 144–159.